ACS APPLIED MATERIALS & INTERFACES

Subscriber access provided by UNIVERSITY OF ADELAIDE LIBRARIES

Article

Solution-Processed Ultrathin TiO2 Compact Layer Hybridized with Mesoporous TiO2 for High-Performance Perovskite Solar Cells

Inyoung Jeong, Yun Hee Park, Seunghwan Bae, Minwoo Park, Hansol Jeong, Phillip Lee, and Min Jae Ko

ACS Appl. Mater. Interfaces, **Just Accepted Manuscript** • DOI: 10.1021/acsami.7b11901 • Publication Date (Web): 09 Oct 2017

Downloaded from http://pubs.acs.org on October 9, 2017

Just Accepted

"Just Accepted" manuscripts have been peer-reviewed and accepted for publication. They are posted online prior to technical editing, formatting for publication and author proofing. The American Chemical Society provides "Just Accepted" as a free service to the research community to expedite the dissemination of scientific material as soon as possible after acceptance. "Just Accepted" manuscripts appear in full in PDF format accompanied by an HTML abstract. "Just Accepted" manuscripts have been fully peer reviewed, but should not be considered the official version of record. They are accessible to all readers and citable by the Digital Object Identifier (DOI®). "Just Accepted" is an optional service offered to authors. Therefore, the "Just Accepted" Web site may not include all articles that will be published in the journal. After a manuscript is technically edited and formatted, it will be removed from the "Just Accepted" Web site and published as an ASAP article. Note that technical editing may introduce minor changes to the manuscript text and/or graphics which could affect content, and all legal disclaimers and ethical guidelines that apply to the journal pertain. ACS cannot be held responsible for errors or consequences arising from the use of information contained in these "Just Accepted" manuscripts.

ACS Publications

ACS Applied Materials & Interfaces is published by the American Chemical Society.
1155 Sixteenth Street N.W., Washington, DC 20036

Published by American Chemical Society. Copyright © American Chemical Society. However, no copyright claim is made to original U.S. Government works, or works produced by employees of any Commonwealth realm Crown government in the course of their duties.

Solution-Processed Ultrathin TiO_2 Compact Layer Hybridized with Mesoporous TiO_2 for High-Performance Perovskite Solar Cells

Inyoung Jeong,[a]‡ *Yun Hee Park,*[b,c]‡ *Seunghwan Bae,*[b] *Minwoo Park,*[d] *Hansol Jeong,*[b] *Phillip Lee,*[b*] *Min Jae Ko*[e*]

[a]Photovoltaic Laboratory, Korea Institute of Energy Research (KIER), Daejeon 34129, Republic of Korea

[b]Photo-Electronic Hybrids Research Center, Korea Institute of Science and Technology (KIST), Seoul 02792, Republic of Korea

[c]KU-KIST Graduate School of Converging Science and Technology, Korea University, Seoul 02841, Republic of Korea

[d]Department of Chemical and Biological Engineering, Sookmyung Women's University, Seoul, 04310, Republic of Korea

[e]Department of Chemical and Engineering, Hanyang University, 222 Wangsimri-ro, Seongdonggu, Seoul, 04763, Republic of Korea

KEYWORDS: perovskite solar cell, electron transport layer, TiO_2, charge recombination, solution process

ABSTRACT

The electron transport layer (ETL) is a key component of perovskite solar cells (PSCs) and must provide efficient electron extraction and collection while minimizing the charge recombination at interfaces in order to ensure high performance. Conventional bi-layered TiO_2 ETLs fabricated by depositing compact TiO_2 (c-TiO_2) and mesoporous TiO_2 (m-TiO_2) in sequence exhibit resistive losses due to the contact resistance at the c-TiO_2/m-TiO_2 interface and the series resistance arising from the intrinsically low conductivity of TiO_2. Herein, to minimize such resistive losses, we develop a novel ETL consisting of an ultrathin c-TiO_2 layer hybridized with m-TiO_2, which is fabricated by performing one-step spin-coating of a m-TiO_2 solution containing a small amount of titanium diisopropoxide bis(acetylacetonate) (TAA). By using electron microscopies and elemental mapping analysis, we establish that the optimal concentration of TAA produces an ultrathin blocking layer with a thickness of ~3 nm and ensures that the m-TiO_2 layer has a suitable porosity for efficient perovskite infiltration. We compare PSCs based on mesoscopic ETLs with and without compact layers to determine the role of the hole-blocking layer in their performances. The hybrid ETLs exhibit enhanced electron extraction and reduced charge recombination, resulting in better photovoltaic performances and reduced hysteresis of PSCs compared to those with conventional bi-layered ETLs.

Introduction

Organic-inorganic lead halide perovskites have been recognized as powerful light harvesters of thin film solar cells and certified power conversion efficiencies (PCEs) as high as 22.1% have been achieved within a few years of their development, which has opened up a new era in optoelectronics.[1-7] Tremendous progress has been made in the performances and stabilities of perovskite solar cells (PSCs) through the identification and optimization of new materials and device architectures as well as in-depth studies of the mechanism of operation of PSCs.[8-19]

The architectures of PSCs are classified as either mesoscopic or planar depending on the presence of a mesoporous electron transport layer (ETL). Planar PSCs are based on a compact layer of an n-type or p-type charge-transporting material, and have the advantages of simple structures, high PCEs, and low-temperature processing. However, most PSCs with high PCEs above 20% have been fabricated with bi-layered TiO_2 ETLs (BI-ETLs) that are composed of a compact TiO_2 thin layer (c-TiO_2) and a mesoporous layer (mp-TiO_2).[20-22] The presence of the mp-TiO_2 layer as a scaffold for perovskite enlarges the surface area of the perovskite absorber and efficiently transports electrons from perovskite to the transparent conductive oxide (TCO) substrate. In addition, the incorporation of the mp-TiO_2 layer can alleviate hysteric behavior in the current density-voltage (J-V) curves of PSCs.[23] The c-TiO_2 layer is essential in both planar and mesoscopic PSCs to block the charge recombination caused by direct contact between the TCO substrate and perovskite.

The electrons passing through the ETL experience resistance at the interface and in the TiO_2 layer.[24, 25] As a result, several attempts have been made to minimize the resistive losses in TiO_2 ETLs. Zhang *et al*. developed consecutive compact and mesoporous (CCM) TiO_2 film as an ETL

of mesoscopic PSCs via one-step spin-coating of TiO_2 paste containing TiO_x precursor solution.[26] With increasing a ratio of TiO_x precursor to paste, macropores are formed in CCM-ETL, which is beneficial for pore-filling of perovskite and it was demonstrated the consecutive structure of TiO_2 ETL could reduce interface resistance and enhance electron transport compared to BI-ETL.[26] Metal doping has been widely used to increase the electrical conductivity of TiO_2 ETLs, and also could modify electronic properties, resulting in a shift in their energy levels.[27-29] Improving the interconnection of the TiO_2 nanoparticles and their adhesion to the substrate can result in efficient charge collection and a reduction in the recombination loss.[30-32] $TiCl_4$ post-treatment is commonly used in dye-sensitized solar cells (DSCs) and has also been applied to PSCs in order to passivate surface traps and enhance the necking of the TiO_2 nanoparticles.[33-35] However, the conventional $TiCl_4$ treatment necessitates an additional sintering process at a high temperature, and the TCO substrate can be damaged by the acidic nature of the $TiCl_4$ solution. Several studies have reported that titanium diisopropoxide bis(acetylacetonate) (TAA) can be used as a binding agent to enhance the cross-linkage between particles and their adhesion to the substrate.[32, 36, 37] K. Wojciechowski *et al*. demonstrated that a low-temperature processable TiO_2 ETL can be prepared by adding a small amount of TAA into the TiO_2 nanoparticle dispersion, and that TAA additive enhances the conductivity and film quality of the resulting TiO_2 ETL.[32]

Reducing the thickness of the c-TiO_2 layer is a simple strategy for improving electron transport to TCO by shortening the pathway within the low conductive TiO_2 layer. In order to be an efficient ETL, the c-TiO_2 layer should be as thin as possible while retaining hole-blocking effectiveness. Atomic layer deposition (ALD) has been used to prepare conformal coatings of ultrathin TiO_2 films as c-TiO_2 layers in PSCs.[24, 38, 39] Li and co-workers controlled the thickness of the c-TiO_2 layer by varying the ALD time and investigated the relationship between the

thicknesses of c-TiO_2 ETLs and the performances of the planar PSCs.[24] They demonstrated that the optimum thickness of the c-TiO_2 layer is 10 nm because of its high transmittance and low charge transfer resistance. Chandiran *et al*. deposited a sub-nanometer TiO_2 layer with ALD onto a spin-coated mp-TiO_2 film and found that a 2 nm thick overlayer is sufficient to block charge recombination at the TCO/perovskite interface.[39] They also suggested that the ultrathin layer could increase the open circuit voltage (V_{oc}) of the PSCs by reduction in the film capacitance of the passivation layer.

Solution processing has the advantages over the vacuum-based ALD technique such as ease of fabrication and low cost. However, the solution spin-coating of few-nanometer TiO_2 layers for PSCs is not generally performed because conventional spin-coating from a sol-gel solution of the c-TiO_2 layer generates pinholes, and the thickness of the spin-coated film should be tens of nanometers (typically ~50 nm) in order to effectively prevent direct contact between perovskite and the TCO substrate.[40]

Herein, we developed a novel mp-TiO_2 single ETL hybridized with ultrathin c-TiO_2 (Hyb-ETL) for high-performance mesoscopic PSCs that can be prepared with a facile one-step solution process from a mp-TiO_2 dispersion containing a small amount of TAA. Electron microscopy and elemental mapping were performed to demonstrate that the presence of TAA results in a sub-nanometer ultrathin TiO_2 layer which completely passivates the surface of substrate that is not covered by TiO_2 nanoparticles. We assessed the effectiveness of the hybrid ETL by comparing its impact on the interface resistances and photovoltaic performances of PSCs with those of an ETL consisting only of a single layer of mp-TiO_2 (compact layer-free, CF-ETL) and a conventional BI-ETL. Due to the reduction in the electron transport distance and the enhancement in the adhesive properties of the mp-TiO_2 layer that result from the addition of

TAA, it was found that the Hyb-ETL enhances electron extraction and reduces charge recombination and thus results in a better photovoltaic performance than the conventional BI-ETL.

Experimental section

Fabrication of hybrid TiO_2 ETLs

mp-TiO_2 paste was prepared by using 30 nm nanocrystalline TiO_2 particles. The anatase TiO_2 nanoparticles were synthesized via the hydrolysis of titanium isopropoxide catalyzed with acetic acid, followed by heating in a sealed autoclave at 230 ^oC for 12 h. Ethyl cellulose, lauric acid, and terpineol were added into the ethanol solution containing the TiO_2 nanoparticles in the following weight ratio: TiO_2/ethyl cellulose/lauric acid/terpineol = 0.18/0.05/0.02/0.75. The ethanol was removed by using a rotary evaporator and the viscous paste was uniformly mixed with a three-roll machine. The lab-made TiO_2 paste was diluted with ethanol (1:3.5, weight ratio) to obtain a mp-TiO_2 dispersion. To prepare a hybrid TiO_2 ETL, a target amount (3, 10, 15, or 25 mol% with respect to Ti) of 0.34 M TAA solution in 1-butanol was added to the mp-TiO_2 solution. The hybrid TiO_2 ETL was fabricated by spin-coating the mixed solution at 3500 rpm for 40 s and heating at 500 ^oC for 30 min.

Fabrication of the perovskite solar cells

Patterned fluorine-doped tin oxide glass substrates (FTO, TEC8, Pilkington) were cleaned by washing with acetone, ethanol, and isopropanol for 20 min and then performing UV-ozone treatment for 20 min. For the conventional bilayer TiO_2 ETLs (BI-ETLs), firstly, a compact TiO_2 layer (c-TiO_2) was coated onto the FTO glass by spin-coating the TAA solution in 1-butanol at 2000 rpm for 40 s, followed by heating at 500 ^oC for 30 min. Then, the mp-TiO_2 solution prepared from the lab-made TiO_2 paste was deposited onto the c-TiO_2 layer with a spin rate of 3500 rpm for 40 s, followed by sintering at 500 ^oC for 30 min. The TiO_2 ETLs without compact layers (CF-TiO_2) were prepared by directly coating mp-TiO_2 layers onto FTO substrates without

a c-TiO_2 layer. Methylammonium lead iodide perovskite ($MAPbI_3$) solution was prepared by dissolving 1 mmol PbI_2 (99.9985%, Alfar Aesar) and methylammonium iodide (Dyesol) in a mixed solvent consisting of dimethyl sulfoxide (DMSO, 99.9% Aldrich) and *N,N*-dimethylformamide (DMF, 99.8%, Alfa Aesar) (1:9, v/v). The perovskite precursor solution was coated onto the ETLs by spin-coating at 1000 rpm for 5 s and then 4000 rpm for 15 s. Diethyl ether was dropped onto the rotating film 7 s before the end of the process and the film was heated on a hot plate at 65 ^oC for 1 min and then at 100 ^oC for 7 min to form a dark perovskite. The hole transport material (HTM) solution was prepared by dissolving 2,2′,7,7′-tetrakis(N,N-p-dimethoxyphenylamine)-9,9′-spirobifluorene (56 mg, spiro-OMeTAD, Merck), 4-tert-butylpyridine (30 mg, 96%, Aldrich), and bis(trifluoromethane)sulfonimide lithium salt (6 mg, 99.95%, Aldrich) in chlorobenzene (1 mL, 99.8%, Aldrich) and deposited by spin-coating at 2500 rpm for 20 s. Finally, 80 nm Au electrode was deposited by thermal evaporation on top of the devices through a mask.

Characterization

The crystal structures of the thin films were characterized with X-ray diffraction (XRD, D/MAX-2500, Rigaku) by using Cu-Kα radiation of 1.541 Å. Cross-sectional images and the surface morphologies of the perovskite films and ETLs were obtained with field-emission scanning electron microscopy (FESEM, Inspect F, FEI). To investigate the interface between the TiO_2 layers and the substrates, ETL-coated glass samples were prepared with the focused ion beam (FIB, Nova 600 NanoLab, FEI) milling technique and characterized by using high angle annular dark field-scanning transmission electron microscopy (HAADF-STEM, Talos F200X, FEI) and elemental mapping. The UV-vis absorbance of the ETLs and perovskites were measured with a

UV-vis spectrometer (Lambda 35, PerkinElmer) in transmission mode. The steady-state photoluminescence (PL) spectra of the samples were recorded by using a Fluorolog3 photoluminescence spectrometer system with a monochromator (iHR320, HORIBA Scientific), and a time-correlated single photon-counting module (TCSPC, consisting of a MPD-PDM Series DET-40 photon-counting detector and a Pendulum CNT-91 frequency counter) was used to carry out time-resolved photoluminescence (TRPL) measurements. An electrochemical analyzer/workstation (CHI600C, CH Instruments, Inc.) was used to perform cyclic voltammetry analysis with a three-electrode configuration by using Ag/AgCl as the reference electrode and a Pt wire as the counter electrode. Electrochemical impedance spectra were obtained by using an impedance analyzer (Solartron 1287) under dark conditions with an applied bias of 0.8 V for frequencies ranging from 1.5 MHz to 100 mHz. Current density-voltage curves were recorded by using a Keithley 2400 source measurement unit and a solar simulator equipped with a 180 W xenon lamp (Yamashida Denso, YSS-50A). A calibrated reference Si solar cell equipped with a KG-3 filter was used to adjust the light intensity to the AM 1.5G 1 sun condition (100 $mWcm^{-2}$). The active area of each cell was measured by using an optical microscope camera (Moticam 1000). External quantum efficiency (EQE) spectra were obtained with the K3100 EQX spectral EQE measurement system (PV Measurements, Inc.).

Results and Discussion

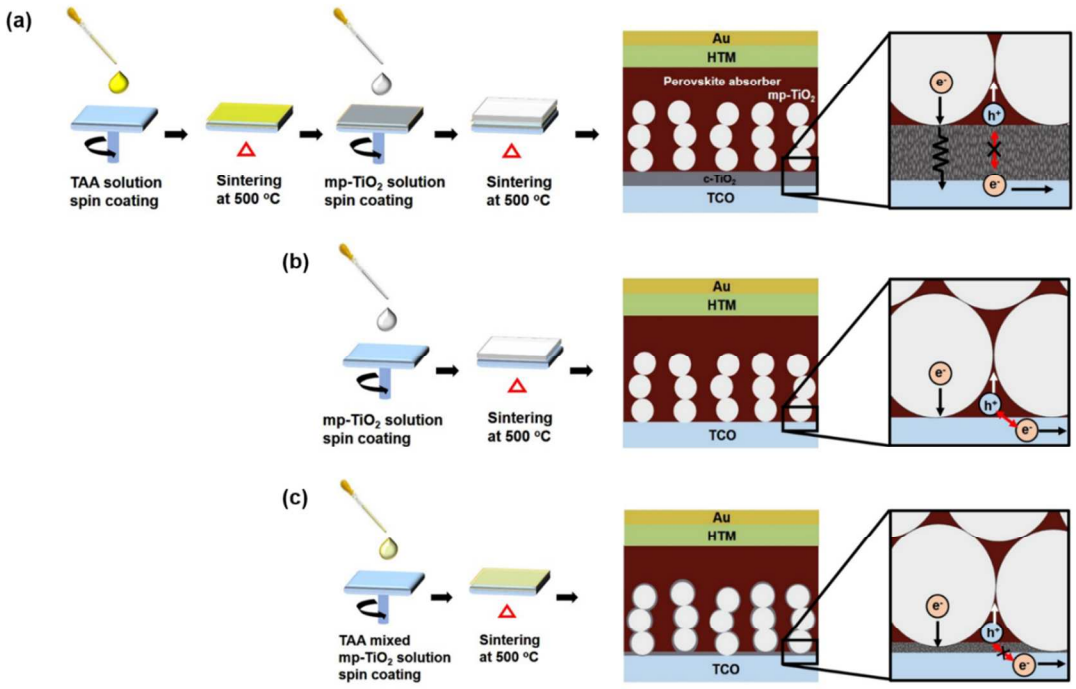

Figure 1. Schematic representation of mesoscopic PSCs based on (a) a BI-ETL, which consists of 50 nm thick c-TiO_2 and 200 nm thick mp-TiO_2 layers, (b) a mp-TiO_2 single layer without a compact layer (the CF-ETL), and (c) an ultrathin TiO_2 compact layer hybridized with mp-TiO_2 (the Hyb-ETL) prepared from a mp-TiO_2 solution containing TAA.

Figure 1 depicts the fabrication processes and structures of the various TiO_2 ETLs studied in this research. A conventional mesoscopic PSC was prepared by firstly spin-coating the TAA solution and subsequent sintering at 500 ^oC to produce the c-TiO_2 layer. Then, the mp-TiO_2 dispersion was coated onto the c-TiO_2 layer, followed by a further sintering process. These two steps produce a bilayer composed of a 50 nm thick c-TiO_2 layer and a 200 nm thick mp-TiO_2 layer (Figure 1a). The compact layer-free PSC was fabricated by depositing an mp-TiO_2 single layer directly onto the substrate in the absence of a c-TiO_2 layer (Figure 1b). To fabricate the Hyb-

ETL, a mp-TiO_2 solution containing a small amount of TAA was deposited onto the TCO substrate with a one-step spin-coating and sintering process. The TAA additive enhances the adhesion of TiO_2 nanoparticles to the TCO substrate and the interconnection between the TiO_2 nanoparticles, which results in an increase in the electrical conductivity of the TiO_2 ETL.[32] In addition, during spin-coating the TAA deposited on the surface of TCO fills the vacant spaces between the mp-TiO_2 nanoparticles, which eventually form an ultrathin TiO_2 compact layer through hydrolysis and crystallization as a result of the thermal sintering process (Figure 1c). As shown in Figure 1, the BI-ETL effectively blocks direct contact between the perovskite absorber and TCO, thereby preventing charge recombination, whereas the CF-ETL-based PSCs are expected to suffer from electron-hole recombination due to the absence of the blocking layer. However, the BI-ETL would exhibit resistive losses due to the contact resistance at the interface between the c-TiO_2 and mp-TiO_2 layers and the series resistance of the low conductivity TiO_2 layer. As shown in Figure 1c, the Hyb-ETL which is an ultrathin TiO_2 layer hybridized with mp-TiO_2 could selectively extract electrons to TCO and minimize resistive losses due to the reduction in the length of the electron transport pathway and its enhanced adhesive properties of the TiO_2 ETL.

We prepared Hyb-TiO_2 ETLs from mp-TiO_2 solutions with various concentrations of TAA (3, 10, 15, and 25 mol% with respect to Ti); unless otherwise noted, the notation Hyb-ETL refers from this point on to the sample derived from the 3 mol% TAA mixed solution, which was found to be the optimal concentration with respect to the photovoltaic performance of the PSC.

The crystal phases of the TiO_2 ETLs were characterized by using X-ray diffraction (XRD). As shown in Figure S1, the diffraction peak at 25.3^o in the XRD pattern of the BI-ETL is assigned to the (101) plane of the anatase phase (PDF no. 21-1272). The Hyb-ETL also reflects anatase

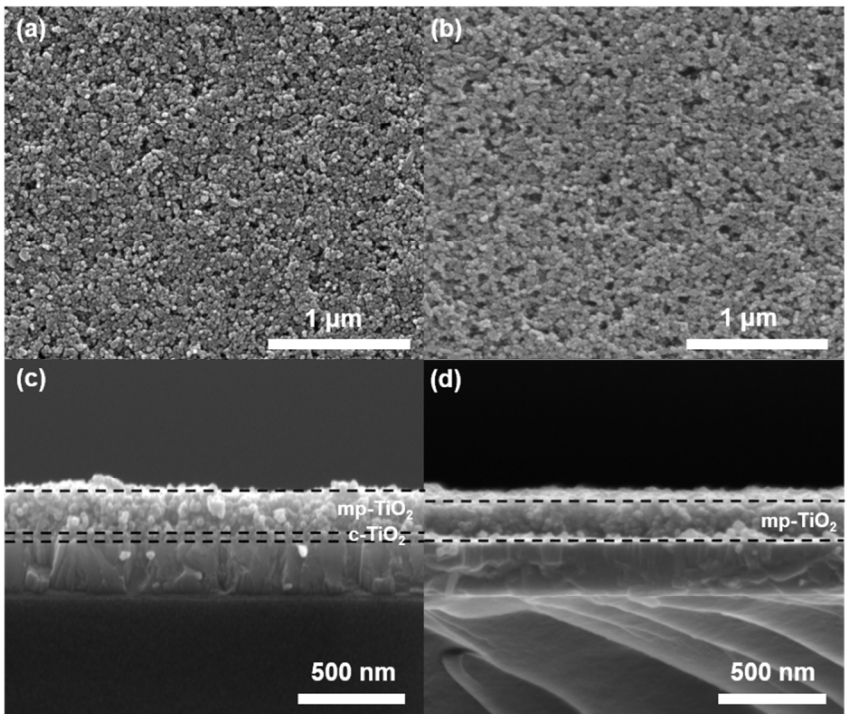

Figure 2. Top-view and cross-sectional SEM images of (a, c) the BI-ETL and (b, d) the Hyb-ETL respectively.

phase without any peaks in its pattern corresponding to the rutile phase. The top-view SEM images in Figure 2a and b show that the addition of a small amount (3 mol% with respect to Ti) of TAA to the mp-TiO_2 solution produces a Hyb-ETL with similar porosity to that of the BI-ETL and no significant alterations in its morphology. The cross-sectional SEM images in Figure 2c and d reveal that the thickness of the BI-ETL is thicker than that of the Hyb-ETL due to the presence of the 50 nm thick c-TiO_2 layer. The c-TiO_2 layer of Hyb-ETL is too thin to observe by SEM. With increases in the concentration of the TAA additive in the mp-TiO_2 solution, it is evident that the porosity and the film thickness of the hybrid TiO_2 ETL gradually decrease (Figure S2). The hybrid TiO_2 ETL containing 25 mol% TAA has the appearance of a compact layer with scant porosity because the many small TiO_2 crystallites derived from TAA fill the pores of the mp-TiO_2 layer. The porosity of the TiO_2 ETL influences the filling fraction of

perovskite within the TiO_2 ETL, and hence on the photovoltaic performance of PSCs based on such ETLs.[26, 41] The low porosity of the mp-TiO_2 layer leads to insufficient infiltration of perovskite and inefficient charge transport, which result in a low open circuit voltage (V_{oc}) and a short circuit current density (J_{sc}).

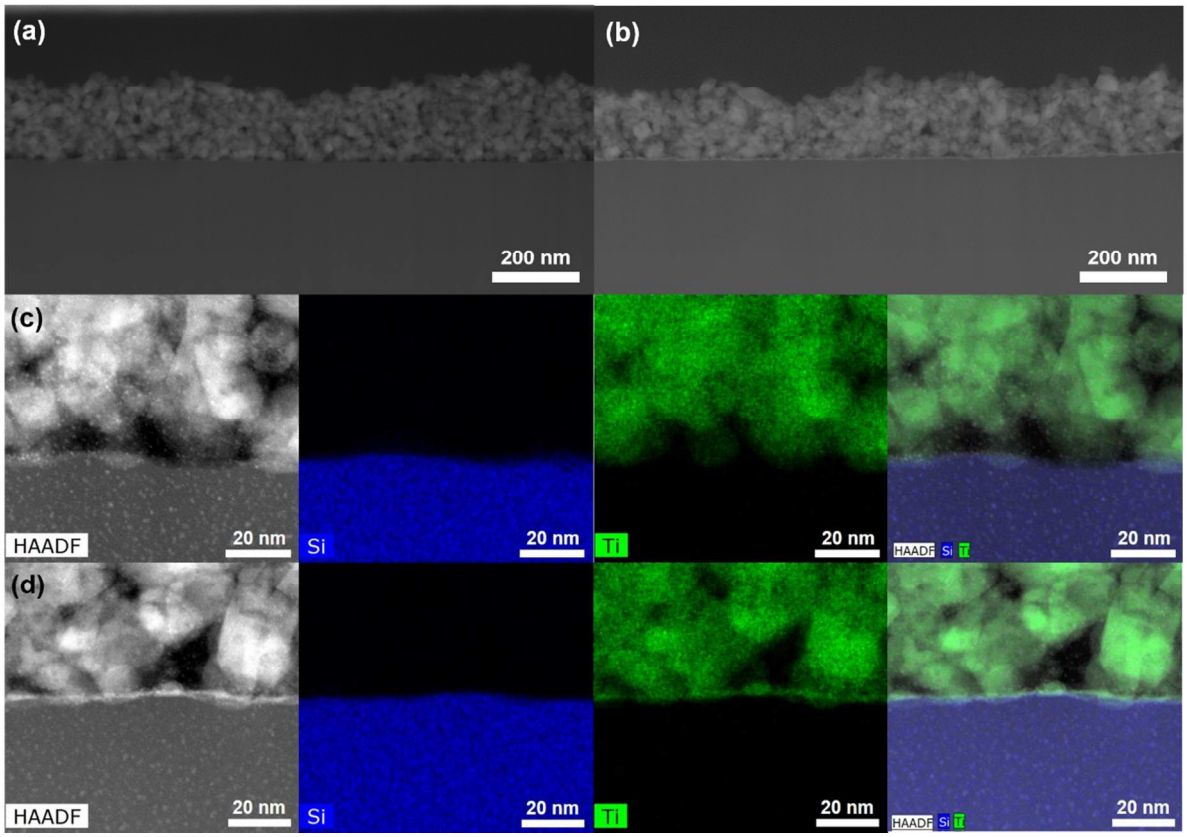

Figure 3. High angle annular dark field-scanning transmission electron microscopy (HAADF-STEM) images and elemental mapping images of (a, c) a CF-ETL and (b, d) a Hyb-ETL coated on glass substrates, respectively.

To closely investigate the interface of the Hyb-ETL with the substrate, we examined cross sections of the mp-TiO_2 ETLs with and without the TAA additive by using the focused ion beam (FIB) milling technique and high angle annular dark field-scanning transmission electron microscopy (HAADF-STEM) combined with elemental mapping analysis. The mp-TiO_2 film

fabricated without TAA (that is, CF-ETL) has exposed parts of the substrate surface which are not covered by TiO_2 nanoparticles (Figure 3a). The TEM images of Hyb-ETL in Figure 3b and Figure S3 provide clear evidences of the presence of ultrathin TiO_2 layer with a thickness of ~ 3 nm, which is in accordance with the corresponding elemental maps of Si and Ti in Figure 3c and 3d. It is expected that the Hyb-ETL with its novel structure covering the whole surface of the substrate will not only effectively block holes but also reduce charge recombination in the associated PSCs, as illustrated in Figure. 1c. To prove the enhancement in interconnectivity of Hyb-ETL, we measured electrical conductivity of the TiO_2 thin films deposited on glass using a 4-point probe set up and the values are summarized in Table S1. We verified that incorporation of small amount (3 and 10 mol%) of TAA increases conductivity compared to pristine TiO_2 film, which is attributed to enhanced interconnection of TiO_2 film. However, the conductivity gradually decreases as the ratio of TAA increased beyond 15% due to the retardation of charge transport caused by many junctions between small crystallites (Figure S2).

Cyclic voltammetry (CV) was used to investigate the blocking effects of the ETLs. As reported previously, TiO_2 does not undergo electrochemical reactions with the ferri/ferrocyanide ($Fe(CN)_6^{3-/4-}$) redox system, i.e. redox reactions occur only at the FTO surface.[40, 42] Therefore, we can compare the hole-blocking capabilities of the different TiO_2 ETLs coated on FTO glass substrates by measuring the current density and peak-to-peak separation (ΔE_P) of the CV curves for $Fe(CN)_6^{3-/4-}$ aqueous solutions. As shown in Figure 4a, the peak current density of the CF-ETL sample is slightly lower than that of the bare FTO substrate, because of the decrease in the number of reaction sites on FTO for $Fe(CN)_6^{3-/4-}$ due to the TiO_2 nanoparticles. The BI-ETL exhibits a lower current density and a larger ΔE_P value than the CF-ETL, which indicates that the 50 nm thick c-TiO_2 layer covers more of the FTO surface. Note that the c-TiO_2 layer prepared

via solution spin-coating doesn't completely cover the whole surface of FTO due to the presence of some pinholes, and thereby it shows a certain current density in the CV curve.[40] We found that the ΔE_P value of the Hyb-ETL, 112 mV, is higher than that of the CF-ETL, 79 mV, and that its hole-blocking capability is comparable to that of the BI-ETL, thus revealing that the 3 nm thick ultrathin layer of the Hyb-ETL is sufficient to effectively block charge recombination. Figure 4b displays the ΔE_P values of hybrid TiO_2 ETL samples fabricated with various TAA additive concentrations. The ΔE_P values of the hybrid TiO_2 ETLs gradually increase with increasing the content of TAA in the mp-TiO_2 solution due to a reduction of porosity as observed in Figure S2.

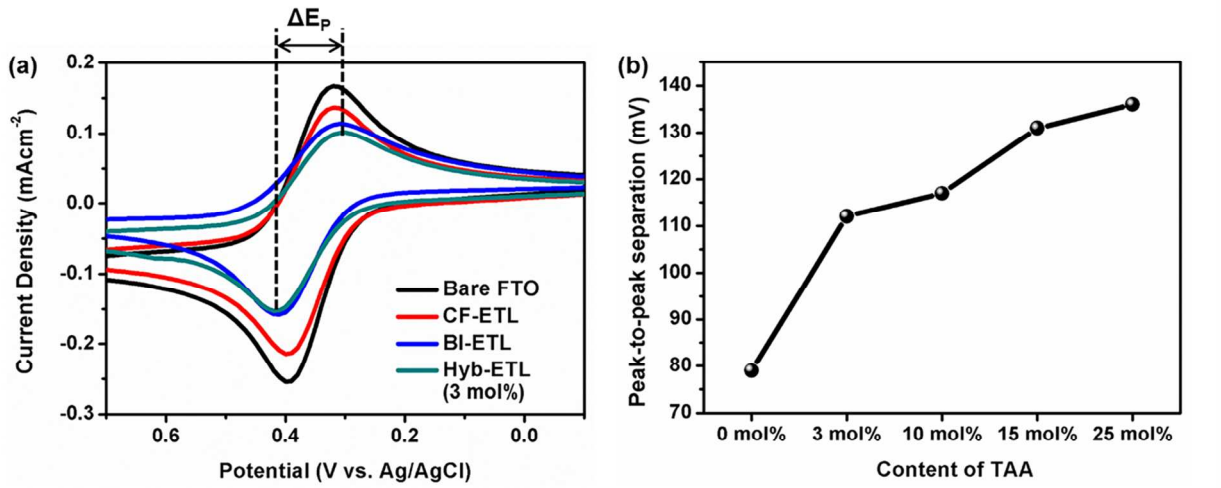

Figure 4. (a) Cyclic voltammetry curves of bare FTO, a CF-ETL, a BI-ETL, and a Hyb-ETL coated onto FTO substrates in $Fe(CN)_6^{3-/4-}$ aqueous solution. (b) Peak-to-peak separation values extracted from the CV data for the hybrid TiO_2 ETLs fabricated from solutions with various TAA contents.

We fabricated uniform and dense methylammonium lead iodide ($MAPbI_3$) perovskite layers by using the adduct-based growth method.[43] The morphology and crystallinity of the perovskite absorber are important factors in the overall photovoltaic performance. The SEM and XRD characterizations in Figure 5a-c show that highly crystalline and dense perovskite layers on the

ETLs were produced and there are no significant differences between the morphologies and crystallinities of the perovskite films on the different ETLs. Figure 5d shows that the absorbances of the perovskite layers on the different ETLs are similar, which is due to the enough light absorption of the thick perovskite capping layer regardless of ETLs. Therefore, it can be concluded that the variation in the photovoltaic performances of the devices mainly originates from the charge extraction and transport properties of the different ETLs.

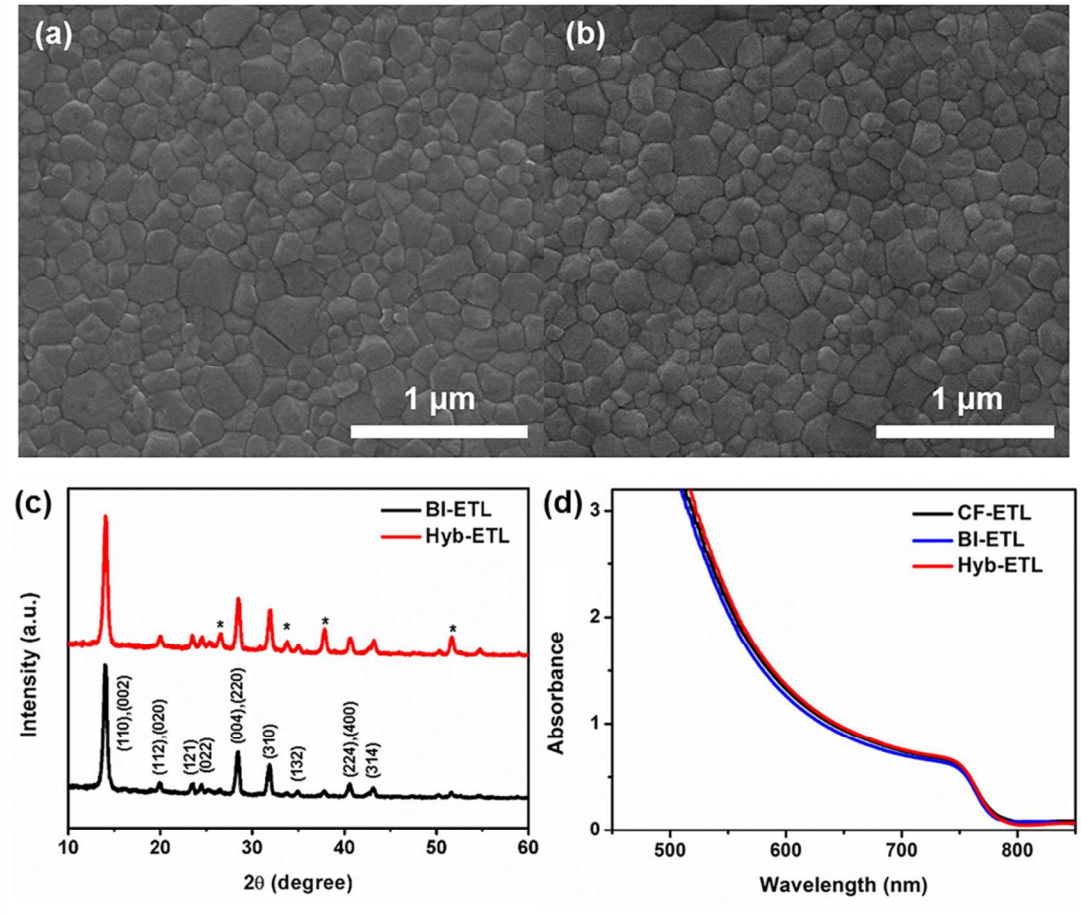

Figure 5. Top-view SEM images of perovskite layers deposited on (a) a BI-ETL and (b) a Hyb-ETL. (c) X-ray diffraction patterns and (d) UV-vis absorbances of perovskite films deposited on the various ETLs. Asterisks denote FTO substrate peaks.

To demonstrate the feasibility of the Hyb-TiO_2 film as an ETL, we fabricated PSCs with the architecture FTO glass/TiO_2 ETL/$CH_3NH_3PbI_3$/spiro-OMeTAD/Au. Figure 6a shows representative current density-voltage (J-V) curves for PSCs based on the CF-ETL, the BI-ETL, and the Hyb-TiO_2 ETL and the corresponding photovoltaic parameters are summarized in Table 1. The CF-ETL-based PSCs exhibited a PCE of 12.89%, a V_{oc} of 1.02 V, a J_{sc} of 19.15 mA cm^{-2}, and a fill factor (FF) of 0.66. The performances of the BI-ETL-based PSCs are superior to those of the PSC without a compact layer: V_{oc} = 1.04 V, J_{sc} = 21.62 mA cm^{-2}, FF = 0.74, and PCE = 16.64%. These results demonstrate that the c-TiO_2 charge selective layer between FTO and perovskite is necessary to prevent recombination and improve the performances of the PSCs. The PSC based on the Hyb-ETL was found to exhibit a J_{sc} of 22.03 mA cm^{-2}, a V_{oc} of 1.06 V, a FF of 0.75, and a PCE of 17.51%. Figure. 6b shows the external quantum efficiency (EQE) spectra of the PSCs based on the different ETLs. The CF-ETL-based device exhibits a low spectral response over the whole visible range due to severe charge recombination. Compared to BI-ETL, the Hyb-ETL-based PSC exhibits higher EQE values, especially at short wavelengths. This result reveals that electron extraction at the interface close to FTO is more efficient for the Hyb-ETL. The integrated J_{sc} values for the PSCs are in good agreement with those obtained from the J-V curves.

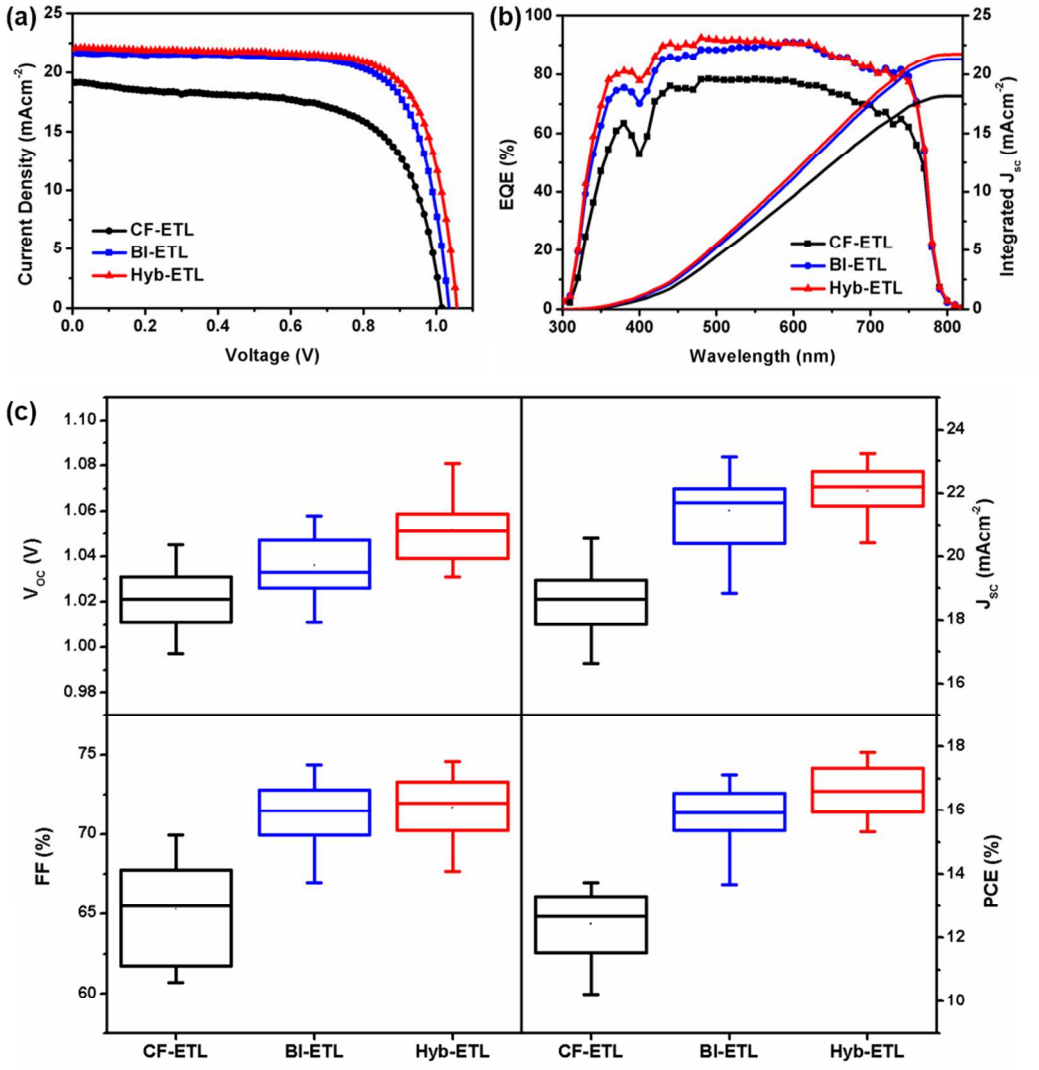

Figure 6. (a) Current density-voltage (J-V) curves and (b) external quantum efficiency (EQE) spectra and integrated J_{sc} of representative PSCs based on CF-ETLs, BI-ETLs, and Hyb-ETLs. (c) The photovoltaic parameters (V_{oc}, J_{sc}, FF, and PCE) of the PSCs based on the different TiO_2 ETLs.

Table 1. Photovoltaic parameters obtained from the current density-voltage curves of representative PSCs based on the various ETLs.

ETL	J_{sc} (mA cm^{-2})	V_{oc} (V)	FF	PCE (%)
CF-ETL	19.15	1.02	0.66	12.89
BI-ETL	21.62	1.04	0.74	16.64
Hyb-ETL	22.03	1.06	0.75	17.51

In order to verify the reproducibility of the devices, we fabricated 25 devices for each ETLs and the average photovoltaic parameters of the devices are displayed in Figure 6c. It can be clearly seen that the higher PCEs of the devices fabricated with the Hyb-ETL compared to BI-ETL stem from increased J_{sc}, FF, and mainly V_{oc}. The improvements for Hyb-ETL are attributed to 1) the improved adhesion of the TiO_2 ETL to the substrate and the improved interconnections between the mp-TiO_2 nanoparticles, and 2) the efficient hole blocking provided by the ultrathin compact layer as well as the reduced electron transport length. When the mixing ratio of TAA is increased above 3 mol%, the photovoltaic performances of PSCs based on hybrid ETLs gradually drop due to decreases in the V_{oc} and J_{sc} values (Figure S5). The drop may be attributed to the insufficient pore filling of perovskite within the mp-TiO_2 scaffold caused by decrease in porosity of ETL. In addition, as shown in Figure S2, the many contact points between the small nanocrystallites derived from TAA retard electron transport and thereby increase electron-hole recombination.

To evaluate the charge extraction in the PSCs based on the BI-ETL and the Hyb-ETL, their steady-state photoluminescence (PL) and time-resolved PL (TRPL) were measured. Figure 7a shows the intrinsic fluorescence emission peak at 765 nm for $CH_3NH_3PbI_3$ and the intensity of the peak of the pristine bare perovskite sample coated on glass is reduced by quenching in the presence of the TiO_2 ETLs. The quenching of the PL of perovskite is greater for the Hyb-ETL than for the BI-ETL. The PL decay transients of perovskite collected at 765 nm after excitation with a 400 nm laser are shown in Figure7b. The PL lifetime of each sample was obtained by fitting the results in Figure 7b by using a bi-exponential decay function, and the fitted parameters are summarized in Table S2. The slow decay time (τ_1) and amplitude (A_1) components are attributed to the recombination of free charge carriers in bulk perovskite, and the fast decay components (τ_2 and A_2) are due to non-radiative recombination and the quenching of charge

carriers by the ETLs.[44] The τ_2 value of the Hyb-ETL-based sample, 1.35 ns, is smaller than that of the BI-ETL/perovskite sample, and the amplitude A_2 is higher (77%), which means that its average lifetime, 5.70 ns, is lower than that (9.04 ns) of the BI-ETL. This result indicates that electron extraction from the perovskite film to the Hyb-ETL is more efficient than that to the BI-ETL, which is consistent with the steady-state PL results.

To investigate the interface charge transport and recombination resistance in the PSCs fabricated with the different ETLs, we performed electrochemical impedance spectroscopy (EIS) in the dark with an applied bias. Figure 7c shows the Nyquist plots of the PSCs based on the BI-ETL and the Hyb-ETL and the equivalent circuit in the inset in Figure 7c was used to fit the Nyquist plots. The series resistance (R_s) is obtained from the intercept of the real part at high frequency. The transport resistance (R_{tr}) in the high-frequency region is associated with carrier transport in the selective layer or at the interface with perovskite.[45, 46] Both devices use the same HTM, so the difference between their R_{tr} values originates from the differences between the TiO_2 ETLs and their interfaces. The recombination resistance (R_{rec}) and the capacitance of the perovskite layer can be determined from the feature appearing at low frequency range of the Nyquist plot.[45-47] As shown in Figure 7c, the first arc at high frequency was indistinguishable and the arcs corresponding to the R_{tr} and R_{rec} component overlap in a depressed arc. The fitted parameters are listed in Table S3. The R_s and R_{tr} values of the Hyb-ETL PSC are 0.71 ohm cm^2 and 84.15 ohm cm^2, respectively and both values are smaller than those (1.80 ohm cm^2 for R_s and 125.13 ohm cm^2 for R_{tr}) of the BI-ETL device. The lower R_s and R_{tr} values of the Hyb-ETL are attributed to the enhanced adhesion of the mp-TiO_2 layer to the FTO glass in the presence of TAA and the reduced electron transport length.

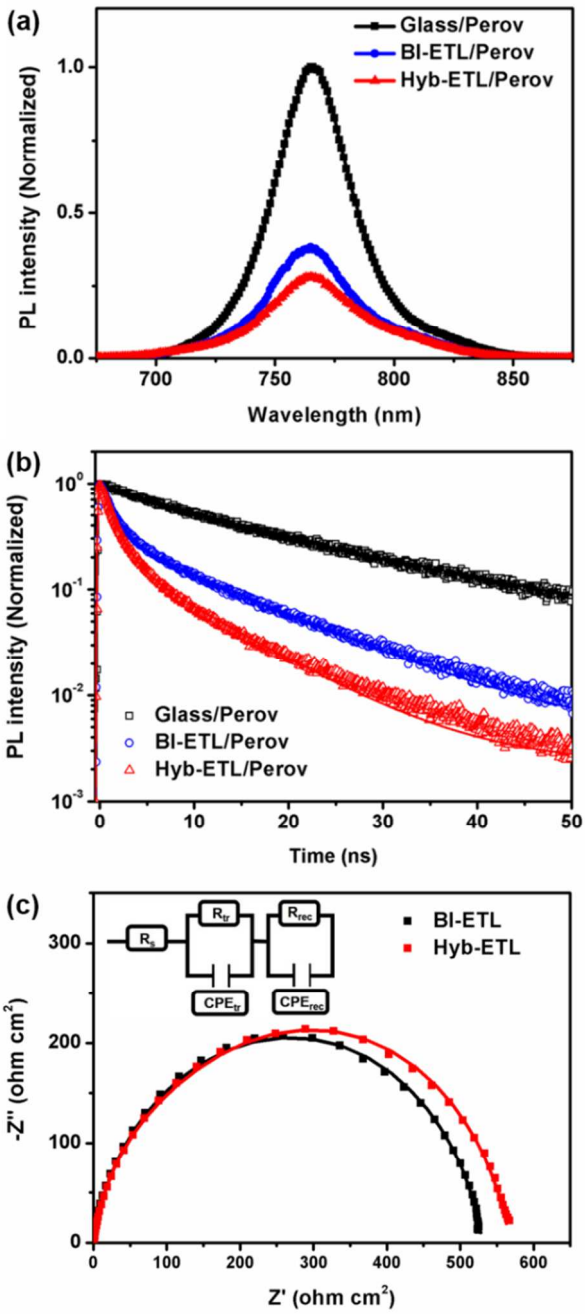

Figure 7. (a) Steady-state photoluminescence (PL) spectra and (b) time-resolved PL (TRPL) spectra of bare perovskite and perovskite layers in contact with a BI-ETL and a Hyb-ETL. (c) Nyquist plots obtained from electrochemical impedance spectroscopy (EIS) results for the BI-ETL- and Hyb-ETL-based PSCs. Symbols: experimental data; Solid lines: fitted data. The inset shows the equivalent circuit used for fitting.

The R_{rec} value of the Hyb-ETL PSC was found to be 483.25 ohm cm^2 which is larger than that of the PSC based on the BI-ETL (405.43 ohm cm^2), indicating that charge recombination is effectively restricted by the Hyb-ETL. The PL and EIS characterizations reveal that the Hyb-ETL-based devices exhibit better V_{oc} and J_{sc} values than the BI-ETL-based devices because of enhanced charge extraction and reduced recombination.

Previous studies have shown that efficient charge extraction in PSCs can suppress hysteresis in J-V curves depending on the scan direction.[27, 48] We compared the hysteresis in the J-V curves of the Hyb-ETL and BI-ETL PSCs at a fixed scan rate of 0.12 $V \cdot s^{-1}$. As shown in Figure 8 and Table 2, the deviation between the J-V curves of the Hyb-ETL-based PSC obtained with forward (from J_{sc} to V_{oc}) and reverse scans (from V_{oc} to J_{sc}) is smaller than that of the BI-ETL-based PSC. The hysteresis index (HI) was calculated by using Equation (1)

$$\text{Hysteresis index} = \frac{J_{RS}(0.8\,V_{oc}) - J_{FS}(0.8\,V_{oc})}{J_{RS}(0.8\,V_{oc})} \qquad (1)$$

where $J_{RS}(0.8\ V_{oc})$ and $J_{FS}(0.8\ V_{oc})$ are the photocurrent densities at the point of 80% V_{oc} for the reverse and forward scans respectively.

The values of HI for the Hyb-ETL- and BI-ETL-based PSCs were found to be 0.035 and 0.051 respectively. The better charge extraction of Hyb-ETL not only improved photovoltaic performance but alleviated hysteric behavior. We also measured the stabilized power output of the Hyb-ETL-based device generated at the maximum power point voltage (0.9 V) to corroborate its performance under real working conditions. Figure S6 shows that it exhibits a steady-state photocurrent of 19.2 mA cm^{-2} and a stabilized PCE of 17.3% under continuous 1 sun illumination, which is close to the PCE value obtained from the reverse scanned J-V curves.

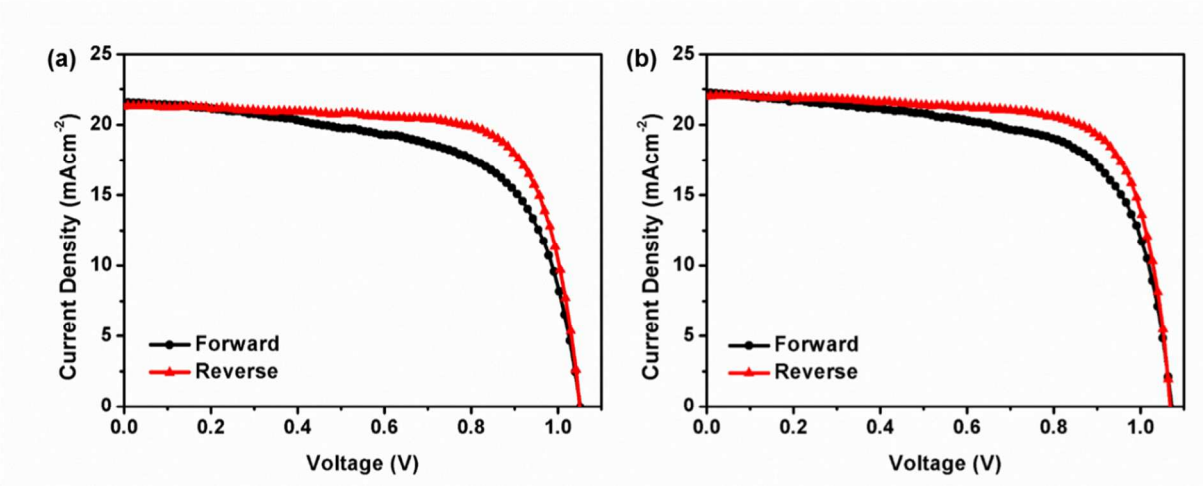

Figure 8. Hysteresis behaviors of the PSCs based on (a) a BI-ETL and (b) a Hyb-ETL in forward and reverse scans (forward: from J_{sc} to V_{oc}; reverse: from V_{oc} to J_{sc}).

Table 2. Photovoltaic parameters of PSCs based on a BI-ETL and a Hyb-ETL for forward and reverse scans.

ETL	Scan direction	V_{oc} (V)	J_{sc} (mA cm^{-2})	FF	PCE (%)	Hysteresis index
BI-ETL	Reverse	1.05	21.28	0.73	16.31	0.051
	Forward	1.05	21.55	0.63	14.26	
Hyb-ETL	Reverse	1.07	22.05	0.74	17.46	0.035
	Forward	1.07	22.26	0.66	15.72	

Conclusion

We have successfully developed solution-processed ultrathin c-TiO_2/mp-TiO_2 hybrid ETL for high-performance mesoscopic PSCs via the one-step spin-coating of a mp-TiO_2 solution containing TAA. The optimal ratio (3 mol%) of TAA in the mp-TiO_2 solution produces an ultrathin hole-blocking layer with a thickness of ~3 nm and an mp-TiO_2 layer with suitable porosity for efficient perovskite infiltration. Compared to a device based on a conventional bi-layered TiO_2 ETL, the Hyb-ETL-based PSC exhibits a higher PCE of 17.51% as well as reduced hysteresis. The superior performance of the Hyb-ETL is attributed to the enhancement of the interconnections between the mp-TiO_2 nanoparticles and the improved adhesion of the mp-TiO_2 layer to the FTO substrate in the presence of TAA, as well as reduced charge transport resistance and recombination. By comparing three types of ETLs (the CF-ETL, the BI-ETL, and the Hyb-ETL) in terms of their hole blocking capability, porosity, and resistive losses in PSCs, their effectiveness as ETLs were assessed. Our solution-phase method not only simplifies the PSC fabrication process but also reduces its cost. This approach can be extended to other metal oxides with high electron mobility and to mixed systems in order to establish favorable energy band alignment for electron extraction and transport.

ASSOCIATED CONTENT

Supporting Information. XRD patterns of TiO_2 ETLs, Top-view and cross sectional SEM images of TiO_2 ETLs, HR-TEM image of Hyb-ETL, SEM images of perovskite layers, Statistics of photovoltaic parameters of devices based on hybrid ETLs with varying mixing concentration of TAA, Fitted parameters of TRPL and EIS, and Stabilized power output of the best-performing device.

AUTHOR INFORMATION

Corresponding Author

* E-mail: phillip@kist.re.kr (P. Lee), mjko@hanyang.ac.kr (M. J. Ko)

Author Contributions

The manuscript was written through contributions of all authors. All authors have given approval to the final version of the manuscript. ‡These authors contributed equally.

Notes

The authors declare no competing financial interest.

ACKNOWLEDGMENT

This work was supported from the Global Frontier R&D Program on Center for Multiscale Energy System (2012M3A6A7054856) and the Technology Development Program to Solve Climate Changes (2015M1A2A2056824) and funded by the National Research Foundation under the Ministry of Science, ICT & Future Planning, Korea; this work was also conducted under the framework of Research and Development of the Korea Institute of Energy Research (B7-2426) and KIST institutional Program.

REFERENCES

(1) Kojima, A.; Teshima, K.; Shirai, Y.; Miyasaka, T. Organometal Halide Perovskites as Visible-Light Sensitizers for Photovoltaic Cells. *J. Am. Chem. Soc.* **2009,** *131*, 6050-6051.

(2) Im, J.-H.; Lee, C.-R.; Lee, J.-W.; Park, S.-W.; Park, N.-G., 6.5% Efficient Perovskite Quantum-Dot-Sensitized Solar Cell. *Nanoscale* **2011,** *3*, 4088-4093.

(3) Lee, M. M.; Teuscher, J.; Miyasaka, T.; Murakami, T. N.; Snaith, H. J., Efficient Hybrid Solar Cells Based on Meso-Superstructured Organometal Halide Perovskites. *Science* **2012,** *338*, 643-647.

(4) Kim, H.-S.; Lee, C.-R.; Im, J.-H.; Lee, K.-B.; Moehl, T.; Marchioro, A.; Moon, S.-J.; Humphry-Baker, R.; Yum, J.-H.; Moser, J. E.; Grätzel, M.; Park, N.-G., Lead Iodide Perovskite Sensitized All-Solid-State Submicron Thin Film Mesoscopic Solar Cell with Efficiency Exceeding 9%. *Sci. Rep.* **2012,** *2*, 591..

(5) Yang, W. S.; Noh, J. H.; Jeon, N. J.; Kim, Y. C.; Ryu, S.; Seo, J.; Seok, S. I., High-Performance Photovoltaic Perovskite Layers Fabricated through Intramolecular Exchange. *Science* **2015,** *348*, 1234-1237.

(6) Brenner, T. M.; Egger, D. A.; Kronik, L.; Hodes, G.; Cahen, D., Hybrid Organic-Inorganic Perovskites: Low-Cost Semiconductors with Intriguing Charge-Transport Properties. *Nat*. *Rev*. *Mater*. **2016,** *1*, 15007.

(7) National Renewable Energy Laboratory, Best Research-Cell Efficiencies chart, www.nrel.gov/ncpv/images/efficiency_chart.jpg (accessed: April, 2017).

(8) Yin, W.-J.; Shi, T.; Yan, Y., Unique Properties of Halide Perovskites as Possible Origins of the Superior Solar Cell Performance. *Adv. Mater.* **2014,** *26*, 4653-4658.

(9) Shin, S. S.; Yeom, E. J.; Yang, W. S.; Hur, S.; Kim, M. G.; Im, J.; Seo, J.; Noh, J. H.; Seok, S. I., Colloidally Prepared La-doped $BaSnO_3$ Electrodes for Efficient, Photostable Perovskite Solar Cells. *Science* **2017**, *356*, 167-171.

(10) Park, Y. H.; Jeong, I.; Bae, S.; Son, H. J.; Lee, P.; Lee, J.; Lee, C.-H.; Ko, M. J., Inorganic Rubidium Cation as an Enhancer for Photovoltaic Performance and Moisture Stability of $HC(NH_2)_2PbI_3$ Perovskite Solar Cells. *Adv. Funct. Mater.* **2017**, *27*, 1605988.

(11) Roiati, V.; Colella, S.; Lerario, G.; De Marco, L.; Rizzo, A.; Listorti, A.; Gigli, G., Investigating Charge Dynamics in Halide Perovskite-Sensitized Mesostructured Solar Cells. *Energy Environ. Sci*. **2014,** *7* , 1889-1894.

(12) Park, N.-G., Methodologies for High Efficiency Perovskite Solar Cells. *Nano Convergence* **2016**, *3*, 15.

(13) Koo, B.; Jung, H.; Park, M.; Kim, J.-Y.; Son, H. J.; Cho, J.; Ko, M. J., Pyrite-Based Bi-Functional Layer for Long-Term Stability and High-Performance of Organo-Lead Halide Perovskite Solar Cells. *Adv. Funct. Mater.* **2016**, *26*, 5400-5407.

(14) Yin, W.-J.; Yang, J.-H.; Kang, J.; Yan, Y.; Wei, S.-H., Halide Perovskite Materials for Solar Cells: a Theoretical Review. *J. Mater. Chem. A.* **2015**, *3*, 8926-8942.

(15) Grancini, G.; Srimath Kandada, A. R.; Frost, J. M.; Barker, A. J.; De Bastiani, M.; Gandini, M.; Marras, S.; Lanzani, G.; Walsh, A.; Petrozza, A., Role of Microstructure in the Electron–Hole Interaction of Hybrid Lead Halide Perovskites. *Nat. Photon.* **2015**, *9*, 695-701.

(16) Mei, A.; Li, X.; Liu, L.; Ku, Z.; Liu, T.; Rong, Y.; Xu, M.; Hu, M.; Chen, J.; Yang, Y.; Grätzel, M.; Han, H., A Hole-Conductor–Free, Fully Printable Mesoscopic Perovskite Solar Cell with High Stability. *Science* **2014**, *345*, 295-298.

(17) Bella, F.; Griffini, G.; Correa-Baena, J.-P.; Saracco, G.; Grätzel, M.; Hagfeldt, A.; Turri, S.; Gerbaldi, C., Improving Efficiency and Stability of Perovskite Solar Cells with Photocurable Fluoropolymers. *Science* **2016**, *354*, 203-206.

(18) Jeong, I.; Jin Kim, H.; Lee, B.-S.; Jung Son, H.; Young Kim, J.; Lee, D.-K.; Kim, D.-E.; Lee, J.; Ko, M. J., Highly Efficient Perovskite Solar Cells Based on Mechanically Durable Molybdenum Cathode. *Nano Energy* **2015**, *17*, 131-139.

(19) Tan, H.; Jain, A.; Voznyy, O.; Lan, X.; García de Arquer, F. P.; Fan, J. Z.; Quintero-Bermudez, R.; Yuan, M.; Zhang, B.; Zhao, Y.; Fan, F.; Li, P.; Quan, L. N.; Zhao, Y.; Lu, Z.-H.; Yang, Z.; Hoogland, S.; Sargent, E. H., Efficient and Stable Solution-Processed Planar Perovskite Solar Cells via Contact Passivation. *Science* **2017**, *355*, 722-726.

(20) Saliba, M.; Matsui, T.; Domanski, K.; Seo, J.-Y.; Ummadisingu, A.; Zakeeruddin, S. M.; Correa-Baena, J.-P.; Tress, W. R.; Abate, A.; Hagfeldt, A.; Grätzel, M., Incorporation of Rubidium Cations into Perovskite Solar Cells Improves Photovoltaic Performance. *Science* **2016**, *354*, 206-209.

(21) Saliba, M.; Matsui, T.; Seo, J.-Y.; Domanski, K.; Correa-Baena, J.-P.; Nazeeruddin, M. K.; Zakeeruddin, S. M.; Tress, W.; Abate, A.; Hagfeldt, A.; Gratzel, M., Cesium-Containing Triple Cation Perovskite Solar Cells: Improved Stability, Reproducibility and High Efficiency. *Energy Environ. Sci.* **2016**, *9*, 1989-1997.

(22) Son, D.-Y.; Lee, J.-W.; Choi, Y. J.; Jang, I.-H.; Lee, S.; Yoo, P. J.; Shin, H.; Ahn, N.; Choi, M.; Kim, D.; Park, N.-G., Self-Formed Grain Boundary Healing Layer for Highly Efficient $CH_3 NH_3PbI_3$ Perovskite Solar Cells. *Nat. Energy* **2016**, *1*, 16081.

(23) Jeon, N. J.; Noh, J. H.; Kim, Y. C.; Yang, W. S.; Ryu, S.; Seok, S. I., Solvent Engineering for High-Performance Inorganic–Organic Hybrid Perovskite Solar Cells. *Nat. Mater.* **2014**, *13*, 897-903.

(24) Lu, H.; Ma, Y.; Gu, B.; Tian, W.; Li, L., Identifying the Optimum Thickness of Electron Transport Layers for Highly Efficient Perovskite Planar Solar Cells. *J. Mater. Chem. A.* **2015**, *3*, 16445-16452.

(25) Choi, J.; Song, S.; Hörantner, M. T.; Snaith, H. J.; Park, T., Well-Defined Nanostructured, Single-Crystalline TiO_2 Electron Transport Layer for Efficient Planar Perovskite Solar Cells. *ACS Nano* **2016**, *10*, 6029-6036.

(26) Zhang, X.-H.; Ye, J.-J.; Zhu, L.-Z.; Zheng, H.-Y.; Liu, X.-P.; Pan, X.; Dai, S.-Y., High Consistency Perovskite Solar Cell with a Consecutive Compact and Mesoporous TiO_2 Film by One-Step Spin-Coating. *ACS Appl. Mater. Interfaces.* **2016**, *8*, 35440-35446.

(27) Jeong, I.; Jung, H.; Park, M.; Park, J. S.; Son, H. J.; Joo, J.; Lee, J.; Ko, M. J., A Tailored TiO_2 Electron Selective Layer for High-Performance Flexible Perovskite Solar Cells via Low Temperature UV Process. *Nano Energy* **2016**, *28*, 380-389.

(28) Peng, J.; Duong, T.; Zhou, X.; Shen, H.; Wu, Y.; Mulmudi, H. K.; Wan, Y.; Zhong, D.; Li, J.; Tsuzuki, T.; Weber, K. J.; Catchpole, K. R.; White, T. P., Efficient Indium-Doped TiO_x Electron Transport Layers for High-Performance Perovskite Solar Cells and Perovskite-Silicon Tandems. *Adv. Energy Mater.* **2017**, *7*, 1601768.

(29) Zhang, H.; Shi, J.; Xu, X.; Zhu, L.; Luo, Y.; Li, D.; Meng, Q., Mg-Doped TiO_2 Boosts the Efficiency of Planar Perovskite Solar Cells to Exceed 19%. *J. Mater. Chem. A.* **2016**, *4*, 15383-15389.

(30) Nanova, D.; Kast, A. K.; Pfannmöller, M.; Müller, C.; Veith, L.; Wacker, I.; Agari, M.; Hermes, W.; Erk, P.; Kowalsky, W.; Schröder, R. R.; Lovrinčić, R., Unraveling the Nanoscale Morphologies of Mesoporous Perovskite Solar Cells and Their Correlation to Device Performance. *Nano Lett.* **2014**, *14*, 2735-2740.

(31) Cha, J.-M.; Lee, J.-W.; Son, D.-Y.; Kim, H.-S.; Jang, I.-H.; Park, N.-G., Mesoscopic Perovskite Solar Cells with an Admixture of Nanocrystalline TiO_2 and Al_2O_3: Role of Interconnectivity of TiO_2 in Charge Collection. *Nanoscale* **2016**, *8*, 6341-6351.

(32) Wojciechowski, K.; Saliba, M.; Leijtens, T.; Abate, A.; Snaith, H. J., Sub-150 °C Processed Meso-Superstructured Perovskite Solar Cells with Enhanced Efficiency. *Energy Environ. Sci.* **2014**, *7*, 1142-1147.

(33) Abdi-Jalebi, M.; Dar, M. I.; Sadhanala, A.; Senanayak, S. P.; Giordano, F.; Zakeeruddin, S. M.; Grätzel, M.; Friend, R. H., Impact of a Mesoporous Titania–Perovskite Interface on the Performance of Hybrid Organic–Inorganic Perovskite Solar Cells. *J. Phys. Chem. Lett.* **2016**, *7*, 3264-3269.

(34) Chen, H.-W.; Huang, T.-Y.; Chang, T.-H.; Sanehira, Y.; Kung, C.-W.; Chu, C.-W.; Ikegami, M.; Miyasaka, T.; Ho, K.-C., Efficiency Enhancement of Hybrid Perovskite Solar Cells with MEH-PPV Hole-Transporting Layers. *Sci. Rep.* **2016**, *6*, 34319.

(35) Liu, Z.; Chen, Q.; Hong, Z.; Zhou, H.; Xu, X.; De Marco, N.; Sun, P.; Zhao, Z.; Cheng, Y.-B.; Yang, Y., Low-Temperature TiO_x Compact Layer for Planar Heterojunction Perovskite Solar Cells. *ACS Appl. Mater. Interfaces*, **2016**, *8*, 11076-11083.

(36) Crossland, E. J. W.; Noel, N.; Sivaram, V.; Leijtens, T.; Alexander-Webber, J. A.; Snaith, H. J., Mesoporous TiO_2 Single Crystals Delivering Enhanced Mobility and Optoelectronic Device Performance. *Nature* **2013**, *495*, 215-219.

(37) Wang, H.-H.; Chen, Q.; Zhou, H.; Song, L.; Louis, Z. S.; Marco, N. D.; Fang, Y.; Sun, P.; Song, T.-B.; Chen, H.; Yang, Y., Improving the TiO_2 Electron Transport Layer in Perovskite Solar Cells Using Acetylacetonate-Based Additives. *J. Mater. Chem. A.* **2015**, *3*, 9108-9115.

(38) Roelofs, K. E.; Pool, V. L.; Bobb-Semple, D. A.; Palmstrom, A. F.; Santra, P. K.; Van Campen, D. G.; Toney, M. F.; Bent, S. F., Impact of Conformality and Crystallinity for Ultrathin 4 nm Compact TiO_2 Layers in Perovskite Solar Cells. *Adv. Mater. Interfaces*. **2016**, *3*, 1600580.

(39) Chandiran, A. K.; Yella, A.; Mayer, M. T.; Gao, P.; Nazeeruddin, M. K.; Grätzel, M., Sub-Nanometer Conformal TiO_2 Blocking Layer for High Efficiency Solid-State Perovskite Absorber Solar Cells. *Adv. Mater.* **2014**, *26*, 4309-4312.

(40) Moehl, T.; Im, J. H.; Lee, Y. H.; Domanski, K.; Giordano, F.; Zakeeruddin, S. M.; Dar, M. I.; Heiniger, L.-P.; Nazeeruddin, M. K.; Park, N.-G.; Grätzel, M., Strong Photocurrent Amplification in Perovskite Solar Cells with a Porous TiO_2 Blocking Layer under Reverse Bias. *J. Phys. Chem. Lett.* **2014**, *5*, 3931-3936.

(41) Leijtens, T.; Lauber, B.; Eperon, G. E.; Stranks, S. D.; Snaith, H. J., The Importance of Perovskite Pore Filling in Organometal Mixed Halide Sensitized TiO_2-Based Solar Cells. *J. Phys. Chem. Lett.* **2014**, *5*, 1096-1102.

(42) Kavan, L.; Tétreault, N.; Moehl, T.; Grätzel, M., Electrochemical Characterization of TiO_2 Blocking Layers for Dye-Sensitized Solar Cells. *J. Phys. Chem. C.* **2014**, *118*, 16408-16418.

(43) Ahn, N.; Son, D.-Y.; Jang, I.-H.; Kang, S. M.; Choi, M.; Park, N.-G., Highly Reproducible Perovskite Solar Cells with Average Efficiency of 18.3% and Best Efficiency of 19.7% Fabricated via Lewis Base Adduct of Lead(II) Iodide. *J. Am. Chem. Soc.* **2015**, *137*, 8696-8699.

(44) Liang, P.-W.; Liao, C.-Y.; Chueh, C.-C.; Zuo, F.; Williams, S. T.; Xin, X.-K.; Lin, J.; Jen, A. K. Y., Additive Enhanced Crystallization of Solution-Processed Perovskite for Highly Efficient Planar-Heterojunction Solar Cells. *Adv. Mater.* **2014**, *26*, 3748-3754.

(45) Li, J.; Li, W.; Dong, H.; Li, N.; Guo, X.; Wang, L., Enhanced Performance in Hybrid Perovskite Solar Cell by Modification with Spinel Lithium Titanate. *J. Mater. Chem. A.* **2015**, *3*, 8882-8889.

(46) W Ke, W.; Zhao, D.; Cimaroli, A. J.; Grice, C. R.; Qin, P.; Liu, Q.; Xiong, L.; Yan, Y.; Fang, G., Effects of Annealing Temperature of Tin Oxide Electron Selective Layers on the Performance of Perovskite Solar Cells. *J. Mater. Chem. A.* **2015**, *3*, 24163-24168.

(47) Yang, D.; Zhou, X.; Yang, R.; Yang, Z.; Yu, W.; Wang, X.; Li, C.; Liu, S.; Chang, R. P. H., Surface Optimization to Eliminate Hysteresis for Record Efficiency Planar Perovskite Solar Cells. *Energy Environ. Sci.* **2016**, *9*, 3071-3078.

(48) Wu, B.; Fu, K.; Yantara, N.; Xing, G.; Sun, S.; Sum, T. C.; Mathews, N., Charge Accumulation and Hysteresis in Perovskite-Based Solar Cells: An Electro-Optical Analysis. *Adv. Energy Mater.* **2015**, *5*, 1500829.

Table of Contents (TOC)